On the contribution of synoptic transients to the mean atmospheric state in the Gulf Stream region

Rhys Parfitt and Arnaud Czaja

Department of Physics, Imperial College London, UK

Abstract

A new decomposition of the time mean sea level pressure, precipitation, meridional velocity and pressure vertical velocity is applied to ERA-Interim reanalysis data over the North Atlantic ocean for the December-February 1979-2011 time period. The decomposition suggests that the atmospheric state over the Gulf Stream is dominated by a continuous series of synoptic systems, or baroclinic waves, propagating across the region. The time mean value of precipitation, meridional and pressure velocities (the latter being taken as a proxy for upward and downward motion) is accordingly set by the propagating waves. The result is particularly striking for the pressure (meridional) velocity considering that ascent and descent (poleward and equatorward flow) could reasonably be expected to cancel out in such a series of waves.

These results shed a new light on analyses of the storm track heat budget in which the residual between diabatic heating and "transient" eddy heat fluxes (singled out through band pass time filtering or spatial Fourier analysis) is interpreted as a Rossby wave source. This interpretation is questioned because, as a consequence of the filtering used, these studies prevent any direct contribution of the "transients" to the time mean pressure or meridional velocity, attributing the latter entirely to the

circulation associated with the thermally forced Rossby wave. The fact that "transients" directly contribute to the observed time mean pressure velocity over the Gulf Stream might also explain the discrepancy between observed and predicted response of the vertical motion field to heating in midlatitudes.

Keywords: Storm tracks, Diabatic heating, Midlatitude climate variability

1 Introduction

Recent studies have revealed the striking presence, in the time mean, of net upward ascent over the Gulf Stream (Minobe et al., 2008). At low levels, the region of ascent is narrow and roughly follows the meandering path of the separated Gulf Stream. The upward motion is less restricted horizontally at mid and upper levels, where it adopts the general southwest to northeast orientation common to many features of the North Atlantic storm-track (e.g., Chang et al., 2002).

These observations are interesting because they support the idea, put forward on many occasions in the literature (e.g., Hoskins and Valdes, 1990; Wilson et al., 2009; Minobe et al., 2008; Czaja and Blunt, 2011), that the Gulf Stream plays a role in shaping the North Atlantic storm track. They are however challenging on at least two accounts. First, with respect to causality. Solely based on observations it is difficult to establish what exactly is the forcing role of the ocean. Modelling work by Minobe et al. (2008), Kuwano-Yoshida et al., (2010), Kirtman et al. (2012) and Brachet et al. (2012) have all suggested that sea surface temperatures (SST) were indeed key to set the pattern of precipitation and the upward motion at low level. However, the impact on precipitation of the large SST gradient associated with the Gulf Stream seems mostly to be me-

diated by the convective parameterizations in these models, with little overall impact on the storms themselves (as measured for example by upward motion at middle to upper levels).

The second challenging aspect of the observations highlighted in Minobe et al. (2008) is that the co-location of time mean upward motion and diabatic heating contradicts the predicted response of the atmosphere to a heat source in the extra-tropics. Indeed, in the seminal study by Hoskins and Karoly (1981), heating is balanced by horizontal advection of cold air in midlatitudes, not by adiabatic expansion in ascent. Transient eddy heat fluxes certainly play a leading order role in the heat budget and were omitted in Hoskins and Karoly's study, which might explain the discrepancy. However, as further work by Hoskins and Valdes (1990) showed, the net condensational heating in the storm track is not opposed entirely by eddy heat fluxes (horizontal and vertical) and there is a clear net residual heat source in the storm track. These findings were recently confirmed by Hotta and Nakamura (2011). It is the purpose of this note to suggest that this issue can be resolved if one acknowledges that the time mean upward motion observed over the Gulf Stream reflects the cumulative effect of synoptic (weather) systems, rather than the response of slower forms of motions to diabatic heating. Key to this proposal is the idea that upward and downward motions do not cancel out in synoptic systems, as had been emphasized in earlier studies (e.g., Green et al., 1966) but, somewhat misleadingly, is often ruled out by construction in analyses where Fourier analysis or time filtering (band pass) is used (e.g., Blackmon et al., 1977).

The paper is structured as follows. In section 2, the data and methods used are presented and the analysis technique applied to sea level pressure, precipitation, meridional motion and pressure velocity in section 3. A discussion is presented in section 4 while conclusions are offered in section 5.

2 Data and Method

This study uses the ECMWF ERA-Interim reanalysis data (Simmons et al., 2007, Berrisford et al., 2009) across a thirty-three year wintertime period (December-February, DJF, 1979-2011). The ERA-Interim reanalysis utilises a 4D-var data assimilation system to incorporate observations over a 12-hour reanalysis period, with forecasts starting at 00:00UTC and 12:00UTC, with spectral resolution T255 ($\sim$0.7^o). Three of the surface variables used here, namely latent heat flux, stratiform precipitation and convective precipitation are not analysed fields and are consequently taken from short-range forecast accumulations. Both surface heat flux and precipitation fields suffer from spin-up during the first few hours of forecast simulation (Kållberg, 2011). However, the magnitude of the spin up difference between 0h-12h and 24h-36h for the net surface energy balance over the GS ($\sim$10Wm^{-2}) is a relatively small fraction compared to the range of daily surface heat fluxes over the GS (e.g. Shaman et al. 2010). For the total precipitation, there is an average spin-up difference of $\sim$0.5mm day^{-1} in the mid-latitude storm track regions. Whilst this represents a larger fraction of the GS precipitation mean than the spin-up fraction for the total heat flux, the relative error still falls within reason (e.g. compared to a total precipitation mean of $\sim$ 4-8mm day^{-1}, as in Minobe et al. (2008)). Small negative values of precipitation caused in the data packing process are set to zero. A "daily instantaneous value" at 12:00UTC is computed for the forecast fields using a 3-hour accumulation from 12:00UTC.

It has been documented that surface heat fluxes over the GS are remarkably variable, a variation that is closely connected to synoptic activity in the overlying atmosphere (Cayan, 1992; Shaman et al. 2010). As a result, analysis in this paper is centred upon a rectangular "GS domain", (-75^{o}W-58.5^{o}W, 31.5^{o}N-

39°N), shown as a black box in Figure 1 and subsequent figures, set to capture the wintertime mean maximum in surface heat flux. A daily air-sea interaction index (ASII) is then defined based on this domain, determined by the amount of surface evaporation within the domain at 12:00UTC, i.e.

$$ASII(t) = \int_{domain} E(x, y, t) dx dy$$

where E is the surface evaporation, x longitude and y latitude.

There are two types of decomposition in this paper, based on deciles of the ASII. In a "ASII decile plot", the relevant variable is averaged at 12:00UTC across each decile, from (a) 0-10% to (j) 90-100%. For example, for a particular variable ω, the plot for the 60-70% decile would be

$$\frac{10}{N} \sum_{ASII=60\%}^{70\%} \omega(ASII)_{1200UTC}$$

in which N is the total number of wintertime days. In a "weighted ASII decile plot", the sum of the daily values at 12:00UTC across a specific decile in ASII is divided by the total 33-year DJF period, subsequently giving the weighted contribution of each decile to the long term mean. For example, the plot for the 60-70% decile would now be calculated as

$$\frac{1}{N} \sum_{ASII=60\%}^{70\%} \omega(ASII)_{1200UTC}$$

A consequence of this is that the sum across (a) 0-10% to (j) 90-100% of a "weighted ASII decile plot" is now equal to the long term mean.

3 Results

3.1 Mean Sea-Level Pressure

Figure 1 illustrates a "ASII decile plot" for anomalies (defined here by the removal of the thirty-three year wintertime mean) in mean sea-level pressure (MSLP). It is clear from this plot that there are no deciles in which the atmospheric state matches that of the mean (identically zero by construction in this case), i.e. there are anomalies present in each decile. As one moves closer towards the extreme deciles (weakest and strongest values of the ASII index), these anomalous patterns appear to shift more strongly towards one of two extreme regimes; that of a high pressure anomaly to the east of the GS domain towards the lower end of the ASII (panels (a)-(b)-(c)), and that of a low pressure system to the east of the GS domain towards the higher end of the ASII (panels (h)-(i)-(j)). Plotting pressure anomalies for each decile as a Hovmöller plot (with "time" taken as the 298 discontinuous indices composing each decile), as in Figure 2, confirms the presence of these two extreme regimes. In each of these cases, there is an opposite pressure anomaly to either side of the GS domain, with the weakest anomaly to the west of the GS. In addition, given that the GS region is an intense region of cyclogenesis, and that Figure 2 confirms there to be significant synoptic activity almost 100% of the time, such a result appears to be consistent with the concept of a baroclinic waveguide constantly propagating across the GS (e.g. Chang et al. 2002).

3.2 Precipitation

The significance of persistent baroclinic activity over the GS is apparent when analysing the total (convective and stratiform) precipitation over the GS. Figure

3 illustrates a "weighted ASII decile plot" for total precipitation. Superimposed on each panel are the associated contours of SST, plotted from 8°C to 26°C at intervals of 2°C. It is interesting to note that these SST contours vary slightly from one decile to the next, indicative of a slight impact of storms on the upper ocean temperature. Once again, there are two opposite regimes present. On those days associated with the passing of a cyclone, there is a localisation of precipitation with the low pressure centre, whilst on those days associated with the passing of an anti-cyclone, the local maximum in precipitation is found to the west of the GS domain, where one finds a developing low-pressure centre regime in Fig. 1(a)-(c). Indeed, this precipitation maximum is expectedly less than those found in a regime with cyclones to the east of the GS domain (panels (h),(i) and (j)), that will have picked up moisture as they travelled across the warm underlying ocean currents through strong surface evaporation fluxes.

3.3 Pressure Velocity and Meridional Motion

Figure 4 illustrates a "weighted ASII decile plot" for low-level (500 hPa) pressure vertical velocity (ω). In NH wintertime, the time mean ω_{500hPa} seen in Fig. 4k meanders with the GS, in agreement with Minobe et al. (2008). Partitioning of the 500 hPa pressure velocity into deciles again suggests the presence of two extreme regimes over the GS. For low deciles (panels (a) to (f)), one observes ascent ($\omega_{500hPa}<0$) on the warm flank of the Gulf Stream (30-40°N,$\sim$ 60°W), while this is replaced by descent for the higher deciles (panels (h) to (j)). Physically, this reflects that large surface turbulent heat fluxes (high deciles) result from a large thermodynamic imbalance between air and water: cold dry air from the land blowing over high SST (i.e. the warm flank of the Gulf Stream) behind the cold front of a low pressure system. Since air subsides behind the cold front, one expects to find high surface heat fluxes co-located with descent

and high SST. Likewise, weak air-sea heat fluxes occur when the warm flank of the Gulf Stream is collocated with the warm sector of a low pressure system. Since upward motion (the warm conveyor) is found there, one indeed expects the low decile panels to show ascent over the warm flank of the Gulf Stream. Partioning of the 900 hPa meridional velocity (v) as in Figure 5 demonstrates analogous patterns as for the 500 hPa pressure velocity. Expectedly, poleward flow is found where one finds ascent and similarly equatorward flow is found where one finds descent.

Consistent with the baroclinic waveguide view in section 3.1 and 3.2, one moves from low to high deciles in Figs. 4 or 5 (i.e., from upper left to lower right panels) in a manner reminiscent of an eastward propagating wave. As mentioned in Section 2, the time mean ω_{500hPa} and v_{900hPa} shown in the bottom left panels in Figs 4 and 5 respectively is, by construction, the sum of all the deciles. Unlike precipitation however, both meridional and pressure velocities can take both positive and negative values, suggesting that the majority of the deciles could effectively "cancel out" in the mean. To test this cancellation quantitatively, we have attempted to reconstruct the time mean pattern in pressure and meridional velocities displayed in Fig. 4k and 5k, respectively, via linear regression analysis. The technique is illustrated in Fig. 6 for v_{900hPa}, in which at each grid point within the domain highlighted in Fig. 5, panel (k), we plot the low ASII decile contribution (grey crosses) and high decile contribution (bold black stars) on the x-axis, as a function of the actual time mean values on the y-axis. In this particular example we chose to test how well the lowest and highest 30-percentiles could reproduce the poleward flow see in the mean in Fig. 5k, so only positive values are considered on the x-axis. It is seen that there is a large scatter when considering the lowest decile, but a better skill with the highest deciles. Actual squared correlation coefficients are given in Table 1 (0 and 0.4

respectively). The combined contribution of these lowest and highest deciles to the mean (i.e., the sum of panels (a)-(b)-(c) and ((h)-(i)-(j), amounting to 60% of the population of days, shown by black circles in Fig. 6) explains about 85% (R^2=0.85) of the spatial pattern seen in the time mean v_{900hPa}. This clearly highlights a non cancellation of the synoptic activity in the two regimes emphasized in previous sections, and their leading contribution to the time mean for v_{900hPa}. This procedure was repeated for equatorward motion at 900 hPa, as well as for $\omega_{500hPa} > 0$ and $\omega_{500hPa} < 0$. It can be seen in Table 1 that for each of these scenarios the correlation with the time-mean does not reduce but rather improves as one adds the two extreme regimes together.

The main conclusion of this analysis is that the time mean ω (now interpreted as a proxy for the upward and downward motion) and v is largely a residual of the upward and downward (northward and equatorward) motion associated with synoptic activity. Indeed, if synoptic activity sets the time mean v at low level, then one would naturally expect to find it also setting the time mean ω, given that much of the associated upward motion derives from low-level wind convergence. Physically, we distinguish two kinds of vertical motion at mid-levels. First, there is the isentropic upglide and downglide (Hoskins et al., 2003) whose dipolar signature is readily seen in Figure 4. This type of vertical motion is expected to provide a large degree of compensation between ascent and descent as the wave propagates eastward. It is also responsible for the smooth, wavy character of the upward velocity field seen in coarse AGCMs (e.g., Bauer and del Genio, 2006; Catto et al., 2010). Second, there is the diabatic contribution to upward motion, which is concentrated into a small part of the synoptic system where condensation is present (Emanuel, 1985). Here, a large amount of precipitation occurs and the flow is rapid and near (moist) adiabatic. Outside it, descent is cloud-free and slow (up to 20 days or more),

determined by radiative heat loss. In this manner, the descending air found in an anti-cyclone trailing behind such a cyclonic system is unlikely to be related in any way to the air that ascended in that system (Green et al., 1966). This second contributor to vertical motion thereby offers much less compensation between ascent and descent.

4 Discussion

The above analysis suggests a new interpretation of the atmospheric time mean heat budget over the Gulf Stream (Hoskins and Valdes, 1990; Minobe et al., 2010; Hotta and Nakamura, 2011). The standard decomposition can be written as,

$$\bar{u}\partial_x\bar{\theta} + \bar{v}\partial_y\bar{\theta} + \bar{\omega}\partial_p\bar{\theta} = \bar{Q} - [\partial_x(\overline{u'\theta'}) + \partial_y(\overline{v'\theta'}) + \partial_p(\overline{\omega'\theta'})] \tag{1}$$

in which the overbar denotes a low pass time average, primes deviations from it (i.e., high frequency transients), θ is dry potential temperature, u is the zonal velocity, v is the meridional velocity, x longitude, y latitude and Q denotes the diabatic heating (the sum of radiative cooling and condensational heating). When linearized around a zonal mean climate, steady Rossby wave solutions for $\bar{u}$, $\bar{v}$, $\bar{\omega}$ can be found in response to the zonally asymmetric component of the residual heating on the right hand side of (1),

$$\overline{Q_{res}} \equiv \bar{Q} - [\partial_x(\overline{u'\theta'}) + \partial_y(\overline{v'\theta'}) + \partial_p(\overline{\omega'\theta'})] \tag{2}$$

Observations suggest a large degree of cancellation in the calculation of $\overline{Q_{res}}$, with low level sensible heating and low to mid-level condensational heating over the warm flank of the Gulf Stream being strongly offset by upward and

poleward heat transport by transient eddies (compare for example Figs. 3c and 3e in Hoskins and Valdes, 1990). Nevertheless, the residual heating, as estimated from the decomposition in (2), is found to be positive and is usually interpreted as a heat source to excite Rossby waves. The analysis in section 3 suggests an entirely different interpretation because the time mean upward motion $\bar{\omega}$ has been inferred to reflect largely the averaging of the upward motion in synoptic systems. It can thus not be interpreted as a response to a residual heating induced by the latter. This explains in a straightforward way why observations of upward motion over a heat source are in contradiction with the theoretical prediction of equatorward and downward flow (Hoskins and Karoly, 1981; Minobe et al., 2010). Clearly, a full assessment of this issue, as well as elucidating the role of the synoptic waves in setting not only $\bar{\omega}$ but also $\bar{v}$ (see section 3.3) in eq. (1), would also require to consider the impact of mechanical forcing by eddy vorticity fluxes on the vertical motion.

More fundamentally, we emphasize that the standard decomposition (1), while exact mathematically, is misleading in terms of causal relationship. By isolating synoptic waves through time filtering, these waves cannot, by construction, contribute to the time mean upward motion (a sum of sine and cosine waves will have a mean of zero –and likewise if spatial Fourier analysis is used to define the transients). Note that this criticism differs from, but also complements, the one usually made with respect to the Eulerian decomposition (1) –namely that transients drive a time mean circulation through momentum and heat fluxes (e.g., Edmon et al., 1980) which is not explicit in (1). A more physically relevant framework might thus be provided by application of residual mean theory to the three dimensional heat budget, possibly following the lines of Hoskins et al. (1983) –see their Appendix A, interpreting their averaging as spatial rather than temporal. To our knowledge this application has not yet been carried out.

Finally, we would like to mention some recent modelling results of relevance to our study, although phrased in a different context (response of the atmosphere to an SST anomaly rather than the time mean atmospheric state). In the study by Smirnov et al. (2015), a change in model resolution was found to cause a different circulation response to the same extra-tropical SST anomaly across the Oyashio Extension. At low resolution, the response of the atmosphere to the imposed warm SST anomaly was found to follow the linear theory of Hoskins and Karoly (1981), with anomalous upward air-sea heat flux opposed by a time mean equatorward flow. At high resolution however, the response was found to be dominated by the transient component of the circulation, and associated with a deep time mean upward motion. Based on our study, we interpret the latter as the cumulative contribution of the upward motion in synoptic waves affected by the SST anomaly (i.e., the model equivalent of the synoptic waves' contribution to the mean which we have attempted at estimating in this study). It is our proposal that such cumulative contribution can only be seen at sufficiently high resolution because it involves a non cancellation between upward and downward motion in storms (see Section 3.3).

5 Conclusions

The main findings of our study can be summarized as follows:

- Baroclinic waves continuously passing over the Gulf Stream make a leading order contribution to the time mean precipitation, meridional and pressure velocities over this region. Although this result is not surprising for precipitation, a positive definite quantity, it is much less so for the pressure and meridional velocities for which motions of both sign could cancel in the mean.

- the net vertical motion over the Gulf Stream is found to be positive (upward) in the winter mean. This is proposed to be the Eulerian signature of the fact that extra-tropical cyclones are fundamentally open systems, with air parcels ascending rapidly in narrow fronts embedded in mobile low pressure systems, the compensating downward motion occurring in a different system or outside the storm track region, in a location possibly quite remote from that of ascent. It must be so over a region of intense air-sea interactions and frontogenesis such as the Gulf Stream because of the large moistening of the atmosphere that these features drive. Indeed, condensational heating is known to concentrate further the ascent in narrow and fast frontal zones and spreads the descending region further horizontally (e.g., Emanuel, 1985).

Our results suggest that the diagnostic studies of the kind championed by Hoskins and Valdes (1990), where the vertical motion is entirely associated with the time mean response to a prescribed heat source, must be interpreted with caution. Rather than acting as a heat source, the effect of synoptic waves on slower forms of motion may be best represented as a downward pull on air parcels outside the narrow frontal zones, a view somewhat reminiscent of that put forward in the Tropics regarding the impact of convection on large scale circulations (e.g., Yanai et al., 1973; Emanuel et al., 1994). This view has interesting implications for understanding the influence of the extra-tropical oceans on storm tracks. It suggests that the key physical process might be the interaction of atmospheric fronts with the underlying SST distribution, and addressing whether this interaction leads to strengthening or a weakening of their upward motion. A recent study by Sheldon et al. (2015) suggests that the Gulf Stream has a strong impact on the transverse circulation at fronts, but more modelling

and observational work is required to address the issue fully.

Acknowledgements

This work is part of R.P.'s PhD funded by the Natural Environmental Research Council. We would also like to thank the ECMWF for allowing access to the ERA-Interim data set. Discussions with Brian Hoskins are also greatly acknowledged.

References

Bauer, M., & Del Genio, A. D. (2006). Composite analysis of winter cyclones in a GCM: Influence on climatological humidity. Journal of climate, 19(9), 1652-1672.

Berrisford, P., D. Dee, K. Fielding, M. Fuentes, P. Kållberg, S. Kobayashi and S. Uppala. The ERA interim archive, ERA Report series 1 (2009).

Blackmon, M. L., Wallace, J. M., Lau, N. C., & Mullen, S. L. (1977). An observational study of the Northern Hemisphere wintertime circulation. Journal of the Atmospheric Sciences, 34(7), 1040-1053.

Brachet, S., Codron, F., Feliks, Y., Ghil, M., Le Treut, H., & Simonnet, E. (2012). Atmospheric circulations induced by a midlatitude SST front: A GCM study. Journal of Climate, 25(6), 1847-1853.

Catto, J. L., Shaffrey, L. C., & Hodges, K. I. (2010). Can climate models capture the structure of extratropical cyclones?. Journal of Climate, 23(7), 1621-1635

Cayan, D. R. 1992. Latent and sensible heat flux anomalies over the northern oceans: Driving the sea surface temperature. Journal of Physical Oceanography, 22 (8), pp. 859–881.

Chang, E. K., Lee, S. and Swanson, K. L. 2002. Storm track dynamics. Journal of Climate, 15 (16).

Czaja, A., & Blunt, N. (2011). A new mechanism for ocean–atmosphere coupling in midlatitudes. Quarterly Journal of the Royal Meteorological Society, 137(657), 1095-1101.

Edmon Jr, H. J., Hoskins, B. J., & McIntyre, M. E. (1980). Eliassen-Palm cross sections for the troposphere. Journal of the Atmospheric Sciences, 37(12), 2600-2616.

Emanuel, K., 1985: Frontal circulations in the presence of moist symmetric stability, J. Atm. Sci., 10, 1062-1071.

Emanuel, K. A., David Neelin, J., & Bretherton, C. S. (1994). On large scale circulations in convecting atmospheres. Quarterly Journal of the Royal Meteorological Society, 120(519), 1111-1143.

Green, J. S. A., Ludlam, F. H., & McIlveen, J. F. R. (1966). Isentropic relative flow analysis and the parcel theory. Quaterly Journal of the Royal Meteorological Society, 92(392), 210-219.

Hoskins, B. J., & Karoly, D. J. (1981). The steady linear response of a spherical atmosphere to thermal and orographic forcing. Journal of the Atmospheric Sciences, 38(6), 1179-1196.

Hoskins, B. J., James, I. N., & White, G. H. (1983). The shape, propagation and mean-flow interaction of large-scale weather systems. Journal of the atmospheric sciences, 40(7), 1595-1612.

Hoskins, B. J. and Valdes, P. J. 1990. On the existence of storm-tracks. Journal of the atmospheric sciences, 47 (15), pp. 1854–1864.

Hoskins, B. J., M. Pedder, and D. W. Johns, 2003: The mega equation and potential vorticity, Quart. J. Roy. Met. Soc., 129, pp. 3277–3303.

Hotta, D., & Nakamura, H. (2011). On the significance of the sensible heat

supply from the ocean in the maintenance of the mean baroclinicity along storm tracks. Journal of Climate, 24(13), 3377-3401.

Kållberg, P. (2011), Forecast Drift in ERA-Interim, Eur. Cent. for Medium-Range Weather Forecasts, Reading, U. K.

Kirtman, B. P., Bitz, C., Bryan, F., Collins, W., Dennis, J., Hearn, N., ... & Vertenstein, M. (2012). Impact of ocean model resolution on CCSM climate simulations. Climate dynamics, 39(6), 1303-1328.

Kuwano-Yoshida, Akira, Shoshiro Minobe, Shang-Ping Xie, 2010: Precipitation Response to the Gulf Stream in an Atmospheric GCM. J. Climate, 23, 3676–3698.

Minobe, S., Kuwano-Yoshida, A., Komori, N., Xie, S. and Small, R. J. 2008. Influence of the Gulf Stream on the troposphere. Nature, 452 (7184), pp. 206–209.

Minobe, S., Miyashita, M., Kuwano-Yoshida, A., Tokinaga, H., & Xie, S. P. (2010). Atmospheric response to the gulf stream: seasonal variations*. Journal of Climate, 23(13), 3699-3719.

Shaman, J., Samelson, R. and Skyllingstad, E. 2010. Air–Sea Fluxes over the Gulf Stream Region: Atmospheric Controls and Trends. Journal of Climate, 23 (10).

Sheldon, L., A. Czaja, B. Vanniere, C. Morcrette, D. Smith and M. Casado, 2015: The Gulf Stream – troposphere connection, Part I: the warm path, submitted to J. Clim.

Simmons, A., S. Uppala, D. Dee, and S. Kobayashi (2007), ERA-Interim: New ECMWF reanalysis products from 1989 onwards, ECMWF Newsl., 110, 25–35.

Smirnov, D., M. Newman, M.A. Alexander, Y.-O. Kwon, and C. Frankignoul (2015): Investigating the local atmospheric response to a realistic shift in the Oyashio sea surface temperature front. J. Climate, 28, 1126-1147.

Wilson, C., Sinha, B., & Williams, R. G. (2009). The effect of ocean dynamics and orography on atmospheric storm tracks. Journal of Climate, 22(13), 3689-3702.

Yanai, M., Esbensen, S., & Chu, J. H. (1973). Determination of bulk properties of tropical cloud clusters from large-scale heat and moisture budgets. Journal of the Atmospheric Sciences, 30(4), 611-627.

	Strongest 30%	Weakest 30%	Combined (60%)
$v_{900} > 0$	0.392	0	0.857
$v_{900} < 0$	0.149	0.402	0.844
$\omega_{500} > 0$	0.050	0.080	0.641
$\omega_{500} > 0$	0.232	0.02	0.524

Table 1: Squared correlation coefficient R^2 of the various linear regressions discussed in the main text.

Figures

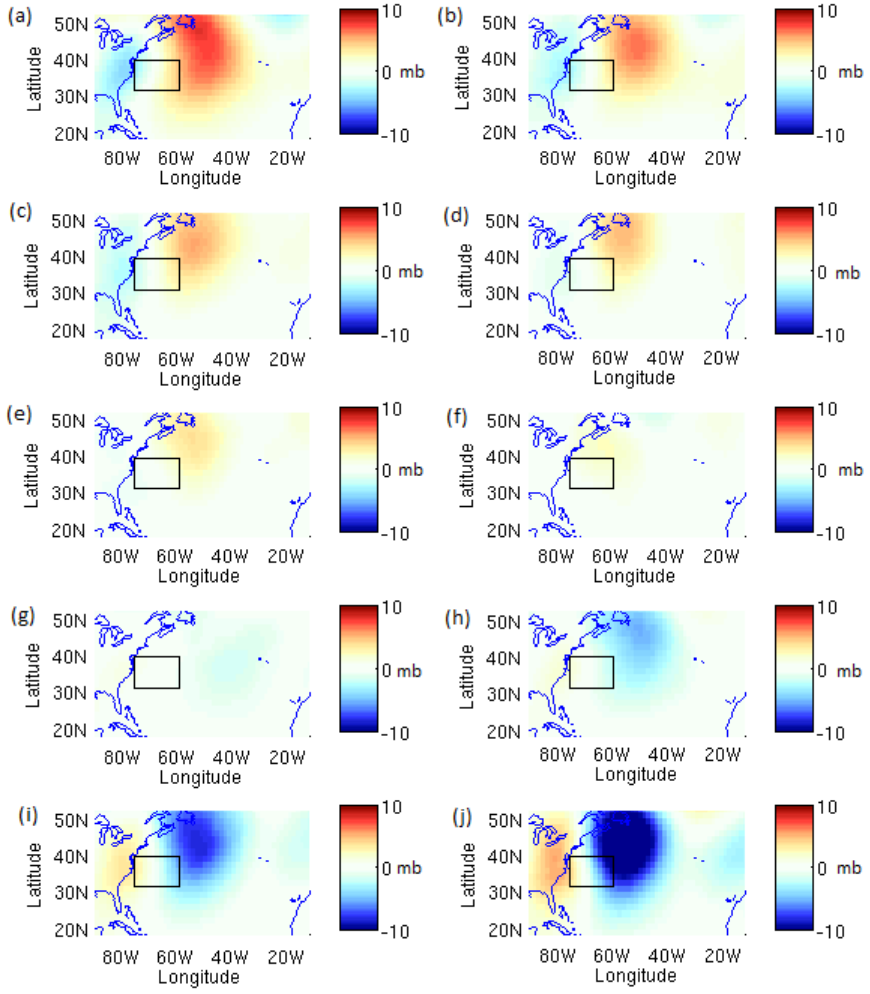

Figure 1: A "ASII decile plot" for sea level pressure. Each panel gives the average sea level pressure anomaly (deviation from the long term wintertime mean) over days corresponding to the (a)0-10% (b)10-20% (c)20-30% (d)30-40% (e)40-50% (f)50-60% (g)60-70% (h)70-80% (i)80-90% (j)90-100% of the population of the ASII index. The coastline is marked in light blue.

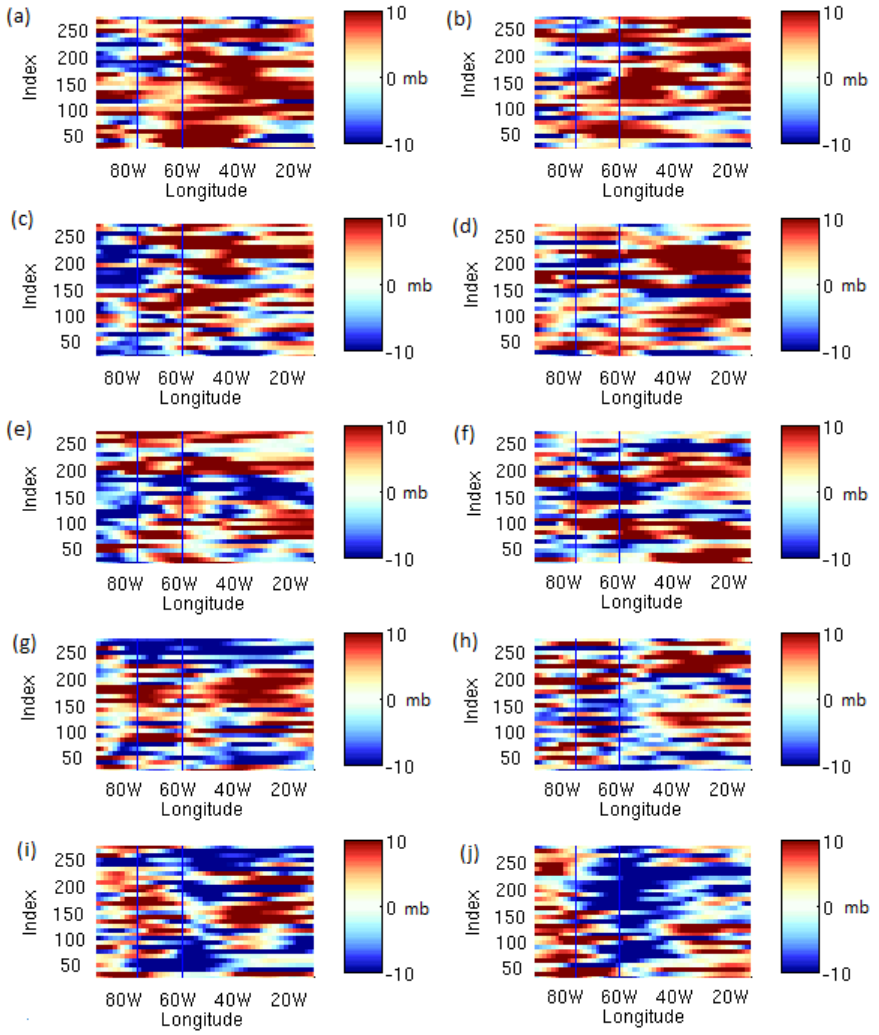

Figure 2: A Hovmöller plot of sea level pressure anomalies in each of the deciles whose mean is shown in Figure 1. On the vertical axis is "time", represented by the 298 discontinuous indices that form each decile. The longitudinal boundaries of the GS domain are plotted as navy vertical lines.

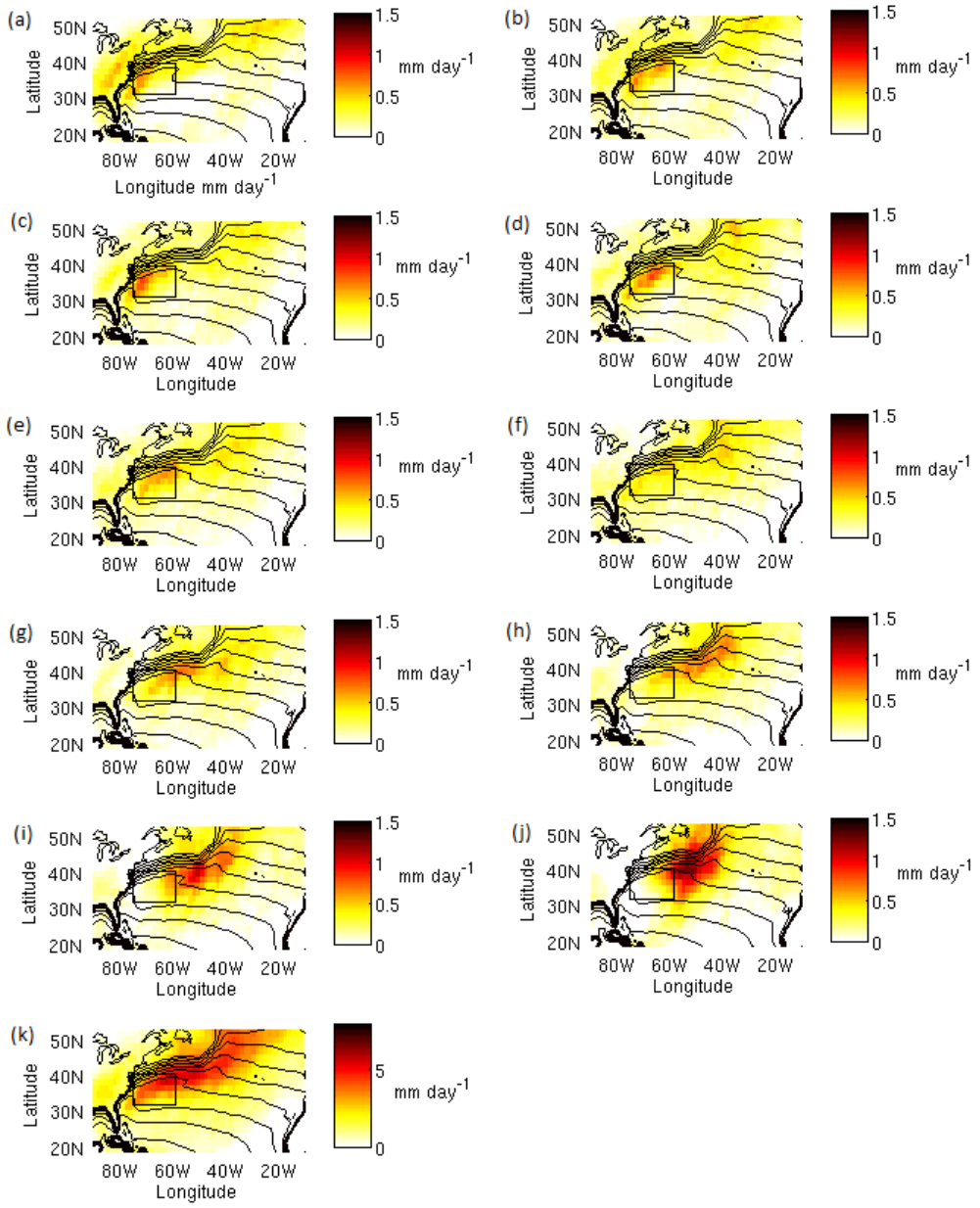

Figure 3: A "weighted ASII decile plot" for total (large scale + convective) precipitation (in mm/day). Note that the bottom left panel (k) is by construction exactly equal to the sum of all panels above it. Thin contours indicate the time mean sea surface temperature (CI = 2K). Note the different colorbar in panel (k).

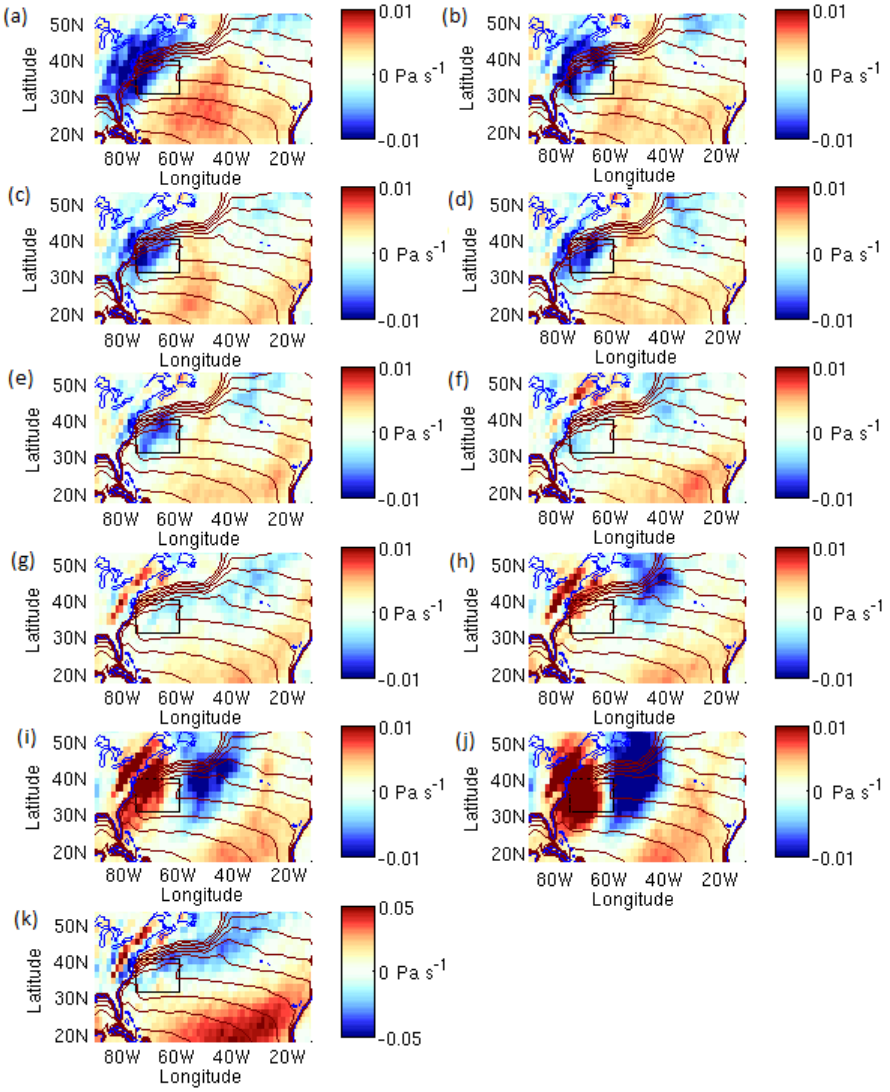

Figure 4: Same as Fig. 3 but for the pressure vertical velocity (ω, in Pa/s) at 500 hPa.

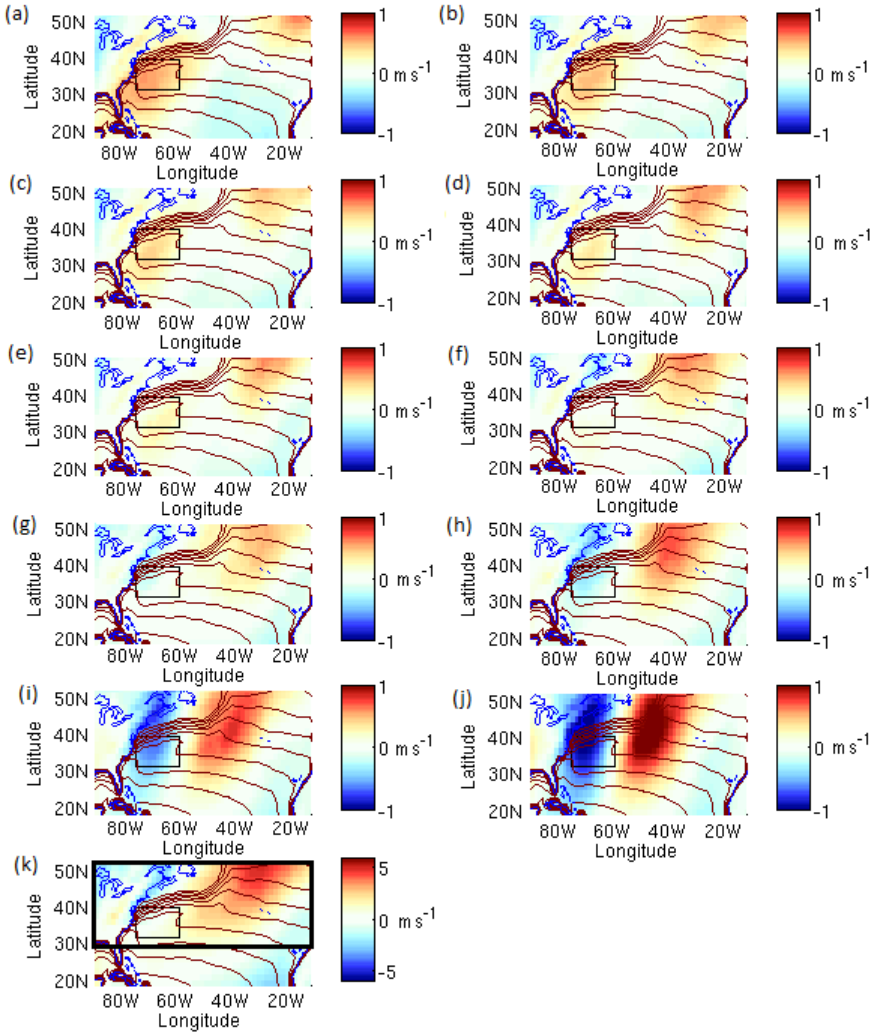

Figure 5: Same as Fig. 3 but for the meridional motion (v, in m/s) at 900 hPa. The black box in panel (k) indicates the domain chosen to reconstruct the time mean field by linear regression.

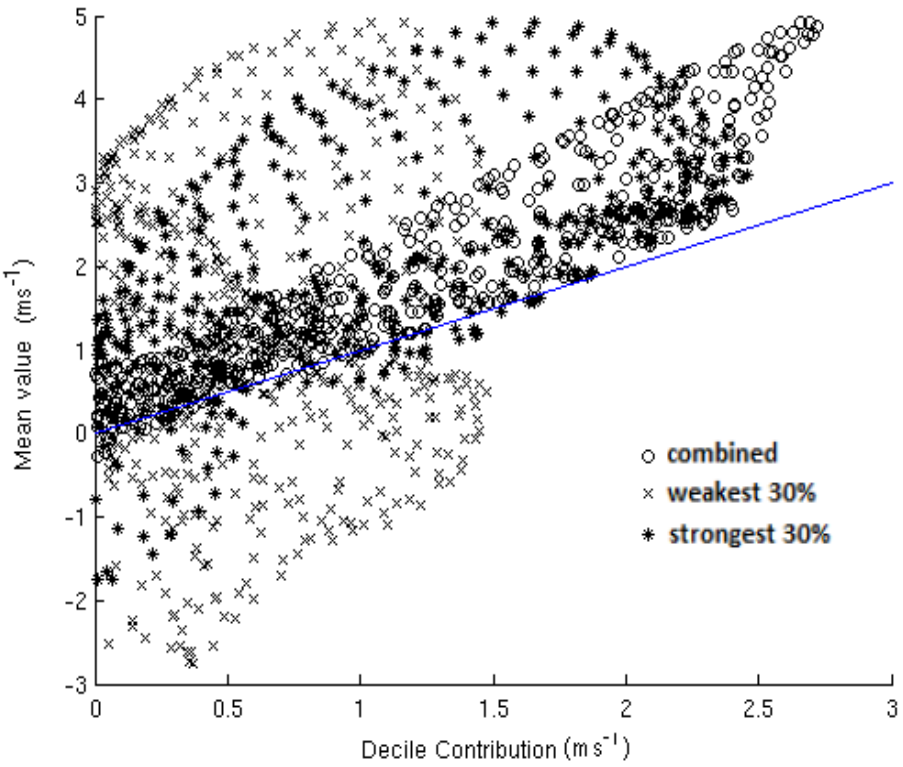

Figure 6: Scatter plot of the poleward components of v_{900} for the strongest 30% in ASII (bold black stars), the weakest 30% in ASII (grey crosses), and the sum of these two extreme regimes (black circles) over the domain (-90°W-10.5°W, 30°N-49.5°N) (marked in Figure 5(k)), each plotted against the values at the respective locations in the time mean.